Backward to Forward Scanning Periodic Leaky-Wave Antenna With Wide Scanning Range

Mohammad H. Rahmani, *Graduate Student Member, IEEE* and Dominic Deslandes, *Member, IEEE*

***Abstract*— A new type of circularly polarized printed periodic leaky-wave antenna (LWA) structure with a wide scanning range and reduced sidelobe level (SLL) is presented. Fifteen matched unit cells (UCs) are cascaded along the direction of propagation to provide seamless frequency scanning from 20 to 29 GHz with a scanning range of 95° from backward to forward quadrant. The open-stopband has been suppressed around the broadside region by matching the input impedance of the UC to the characteristic impedance of the transmission line. Two empirical transmission line models are presented to describe the behavior of the periodic LWA. Parametric study using full-wave simulation is used to improve the SLL and minimize the axial ratio of the circular polarization leading to a fully optimized periodic leaky LWA.**

***Index Terms*— Backward to forward scanning, broadside radiation, circular polarization, open-stopband (OSB), periodic leaky-wave antenna (LWA).**

I. Introduction

PRINTED microstrip antennas have been widely used in various microwave projects due to their low profile, ease of fabrication, and low cost. On the other hand, leaky-wave antennas (LWAs) have the unique feature of radiation beam scanning by changing the frequency of the input signal [1]–[3]. As opposed to resonant antennas, the leakage of traveling waves along the antenna length causes the radiation in LWAs [1]. Because of the frequency dependence of the phase constant (i.e., β), the direction of the radiation beam changes with the frequency, hence producing a frequency scanning antenna.

LWAs can have a uniform geometry or be composed of a cascade of unit cells (UCs) [1], forming a periodic antenna. The main distinction between uniform and periodic LWAs is in their dominant mode which is a fast radiating wave in the uniform structure and a slow wave in periodic structures that does not radiate. However, the periodic repetition of the UCs in the periodic LWA produces an infinite number of space harmonics that can be fast or slow. The fast harmonics are then responsible for the radiation [1], [3]. Usually, one space harmonic is sufficient to represent the propagation constant of a periodic structure [3] (usually $n = -1$ space harmonic). β_{-1} can vary from a negative value to a positive one which results in backward to forward scanning of the radiation pattern.

Manuscript received June 8, 2016; revised April 5, 2017; accepted May 5, 2017. Date of publication May 17, 2017; date of current version July 1, 2017. *(Corresponding author: Mohammad H. Rahmani.)*

The authors are with the Department of Electrical Engineering, École de Technologie Supérieure, Montreal, QC H3C1K3, Canada (e-mail: mohammadhassan.rahmani.1@ens.etsmtl.ca; dominic.deslandes@etsmtl.ca).

Color versions of one or more of the figures in this paper are available online at http://ieeexplore.ieee.org.

Digital Object Identifier 10.1109/TAP.2017.2705021

Several parameters may limit the scanning range of a periodic LWA. The requirement of only one radiating space harmonic in the radiation range, impedance matching bandwidth of the single UC, the open-stopband (OSB), and the relative permittivity of the dielectric are design parameters to consider in order to have a broadband scanning feature [3]–[7]. In order to increase the bandwidth and the scanning range of the antenna at the same time, optimized UC matched through the whole scanning range should be used with a relatively low permittivity and a single space harmonic in the radiation region [3]–[7].

Various methods have been proposed to eliminate the OSB and perform a scan that includes the broadside [4], [6], [8]–[12]. Metamaterial-based transmission line composite right/left hand (CRLH) in frequency-balanced [13]–[15] and Q-balanced [13], [14] configurations has been suggested to suppress the OSB. In a frequency-balanced metamaterial transmission line, the shunt and series branches resonate at the same frequency [13]–[15] while in a Q-balanced transmission line the series and shunt quality factors are equal resulting in the suppression of the OSB. However, the design and fabrication of a balanced CRLH structure at high frequency is not a straightforward task. Moreover, these structures are very sensitive to fabrication and measurement inaccuracies that usually occur in this frequency range [8], [16]. Another method proposed to eliminate the OSB is to use an impedance transformer in the comb-shaped periodic antenna with the radiation occurring at $n = -1$ space harmonic [9]. This method is based on the fact that at the OSB frequency, the input impedance matching is poor and the Bloch impedance has a high imaginary value [17]. Hence, a quarter-wavelength transformer is used to match the Bloch impedance to the line impedance at the broadside and eliminate the OSB [9], [10]. This method, however, uses an impedance matching transformer in every period, increasing the length of the antenna. In order to solve the size problem, the use of a matching stub and a delay line near the radiating stub instead of the impedance transformer has been proposed [9]. However, this structure has a scanning range of about 12°. This bandwidth and scanning range are not enough for wideband applications.

The effect of UC asymmetry on the broadside radiation and the antenna polarization has been fully investigated in [18]–[20]. It has been proved in [20] that the axial asymmetry of the UC produces an elliptical polarization which is due to the quadrature phase relation between the series and shunt radiation contributions. Therefore, inserting an axial asymmetry in the UC leads to circular polarization which is desired for many applications such as radars and satellite

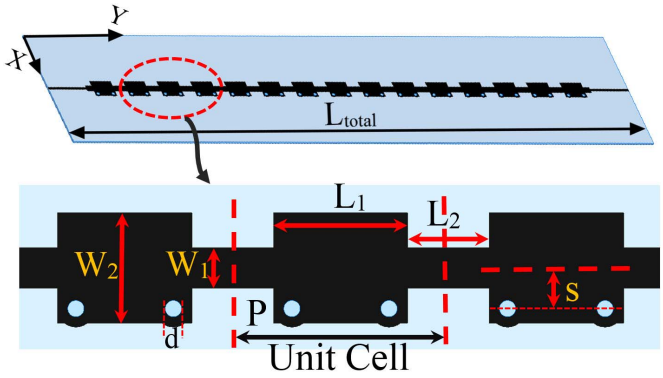

Fig. 1. Periodic LWA structure.

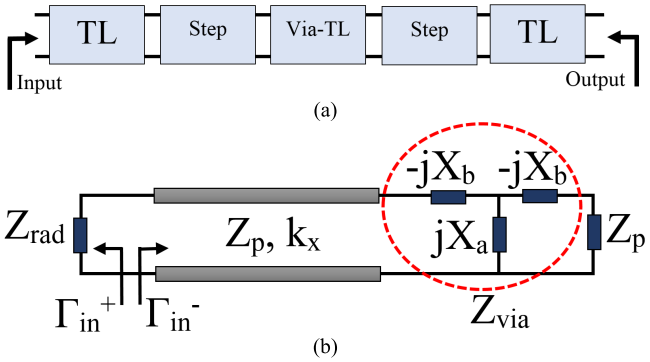

Fig. 2. UC Model. (a) Decomposed two ports network model of the UC. (b) Proposed TEN for the transmission line with vias.

communications. Although the main focus of this work is circular polarization, the scanning range that is presented in this paper is very limited ($+6°$ to $-6°$). Moreover, it uses 40 UCs and has a length of 22λ which is considered a large antenna. One of the presented antennas in [20] is a series-fed patch antenna. This structure was first introduced in [21] and has a limited impedance bandwidth of 6% caused by the narrow bandwidth of the single resonator.

In this paper, we propose a new type of 1-D circularly polarized periodic LWA using periodically distributed UCs composed of two step discontinuities and two shorting vias with improved sidelobe level (SLL), wideband impedance matching, and wide scanning range (Fig. 1). The relatively low $\varepsilon_r = 6.15$ chosen for this structure results in a higher fundamental group velocity [3] which in turns lowers the scanning sensitivity of the antenna (i.e., the slope of β_{-1} versus frequency). This allows for the scanning to occur over a larger frequency range and leads to higher antenna efficiency [5], [6]. In order to increase the impedance bandwidth of the periodic LWA, the wideband UC is self-matched with $Z_0 = 50\ \Omega$ over the desired frequency band making it needless of a separate matching circuit. By doing this, we ensure that the periodic repetition of the UCs will still be matched over the bandwidth. Therefore, the seamless backward to forward scanning feature along with the matched UC over the bandwidth, provides a wideband impedance adaptation of the periodic LWA with a wide scanning range provided by the low relative permittivity of the substrate (i.e., $\varepsilon_r = 6.15$). The axial asymmetry caused by the vias on the UC of this LWA provides a near circular polarization. It will be shown that by following the optimization procedure presented in [20]; it is possible to achieve a circular polarization with an acceptable axial ratio. The UC is designed and optimized with an analytical model to remove the OSB and further investigated using a computer-aided method to minimize the SLL and optimize the axial ratio of the circular polarization. The final structure is one layered, compact, has a simple structure, and provides a wide scanning range.

The structure of this paper is as follows. In Section II, an empirical transmission line model is obtained for the UC in order to predict its behavior and characterize its dispersion properties. Section III is dedicated to the antenna design process where a parametric study of the UC is performed and more details are given about the design of the periodic LWA. In this section, the tapering of the UC in order to lower the SLL of the antenna is presented. Moreover, the circular polarization and axial ratio optimization of the antenna are investigated and discussed in this section. Finally, the measurement results of the uniform and tapered antennas are compared with simulations in Section IV.

II. Theory and UC Analysis

The proposed periodic LWA structure is presented in Fig. 1. This antenna is composed of a periodic repetition of a UC along the direction of propagation. The UC is composed of a microstrip line with a characteristic impedance of Z_0 which is loaded by two step discontinuities and two shorted vias.

The periodic LWA can be analyzed as a series-fed array antenna [22]. The advantage of such analysis is that each UC represents an element of the array that needs to have a good impedance matching and radiation performance. Moreover, by using the array factor analysis, the final radiation pattern of the antenna can be predicted using the single element factor and the complex propagation constant of the periodic structure [22].

The Bloch wave analysis is used to obtain the dispersion characteristics of this periodic structure. The propagation constant of the periodic structure is obtained using the infinite periodic structure formulation in [23]

$$\gamma = 1/P\left(\cosh^{-1}\frac{A+D}{2}\right) \tag{1}$$

where $\gamma = \alpha + j\beta$, A and D are the transmission parameters of the single UC and P is the period. This method gives us the attenuation and phase constant of an infinitely long structure.

In order to find the transmission parameters of a UC, an analytical method based on transmission line theory and transverse equivalent network (TEN) [24] is proposed. In this model, the UC is decomposed into a cascade of two-port networks shown in Fig. 2(a). The total transmission parameters are then obtained from cascading the parameters of each block.

The model is composed of the two microstrip transmission lines, two steps, and a transmission line with two vias. The transmission parameters of the microstrip line are well known and can be found in [23]. In the following sections, the model

for the microstrip line with vias and the discontinuities will be obtained.

A. Transmission Line With Vias on the Side

In order to model this section of the UC, the TEN method is used. The proposed TEN is shown in Fig. 2(b). It is composed of a transmission line with the characteristic impedance Z_p and wavenumber k_x, Z_{rad} which represents the radiating edge of the transmission line and Z_{via} that characterizes the two vias on the other side. Markuvitz [25] proposed a model for a row of metallic vias in a waveguide that can be used for this structure since the vias are far enough ($P/d > 5$). This model is a T network which is composed of two series capacitors and one parallel inductor with the respective inductances (X_a and X_b). On the other hand, Z_{rad} is defined using the truncated transmission line approximation given in [26]

$$Z_{\text{rad}} = jZ_p \cot\left(\frac{\chi(k_y)}{2}\right)$$
$$Z_p = \frac{\omega\mu_0}{k_x}. \tag{2}$$

where k_y is the wavenumber in the direction of propagation and $\chi(k_y)$ can be obtained using the formula presented in [26]. Once the values of Z_{via} and Z_{rad} are known, the TEN is complete and the complex propagation constant (k_y), and consequently the transmission parameters of this section can be obtained by solving the transverse resonance equation

$$\Gamma_{in}^{+}(k_y) \times \Gamma_{in}^{-}(k_y) = 1. \tag{3}$$

B. Modeling the Discontinuities

Due to the presence of the vias at the discontinuities, the well-known formulations for modeling a step discontinuity presented in [27] cannot be directly used. Two methods are proposed to solve this problem.

1) Model 1: The first method consists of modeling the wide line with vias with a half-width microstrip line. As it is demonstrated in [28], a half-width microstrip line can be replaced with a full-width microstrip line with the first higher order mode (EH_1) propagating in it. Then, the characteristic impedance of this line can be found using the waveguide model presented in [29]

$$Z_2 = 8\eta_0 \sin^2\left(\frac{\pi W_2}{w_{eff}}\right)\frac{k_0 h}{\beta_{lw} w_{\text{eff}}}\sqrt{\frac{\mu_r}{\varepsilon_r}}$$
$$w_{\text{eff}} = h\left[\frac{W_2}{h} + \frac{2}{\pi}\ln\left(2\pi\exp\left(\frac{W_2}{2h} + 0.92\right)\right)\right] \tag{4}$$

where ε_r is the relative permittivity of the dielectric, μ_r is the relative permeability of the dielectric, h is the height of the substrate, $\eta_0 = 120\ \pi$, and β_{lw} is the phase constant of the line with vias. Now by inserting this new impedance in the formulations presented in [27], the T network of the discontinuity can be approximated. With this approximation, the accuracy of the model is limited. However, it can be used as a first step of the design process to understand the behavior of the UC.

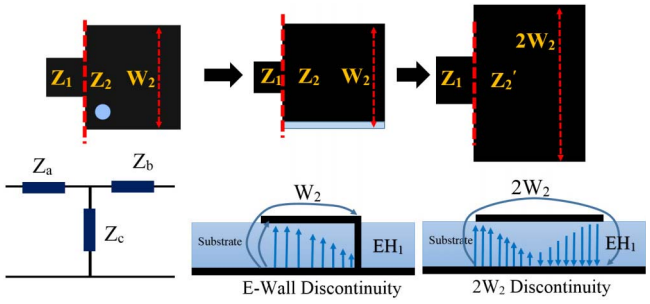

Fig. 3. Discontinuity modeling by replacing the impedance of the second line by the impedance of a double width microstrip line with EH_1.

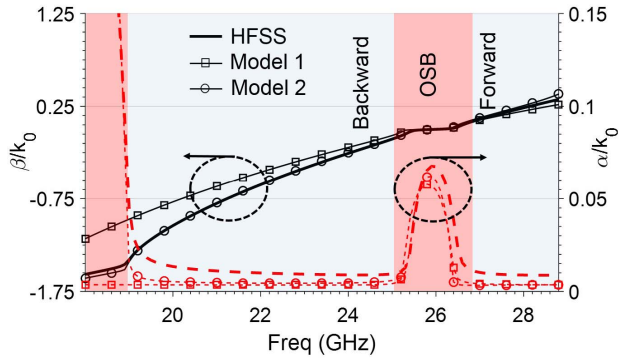

Fig. 4. Dispersion characteristics of the nonoptimized UC with $\varepsilon_r = 6.15$ and $h = 250\ \mu$m. The solid lines represent the phase constant and the dashed lines represent the attenuation constant.

2) Model 2: In order to obtain a more accurate solution, a second method based on curve fitting is deployed. In this method, simulations were performed using a commercial electromagnetic solver (HFSS) [30] to extract different curves for the variations of the T network impedances (Z_a, Z_b, and Z_c) shown in Fig. 3. Related functions for the T network are obtained for different values of W_2 as a function of frequency by fitting all these curves using the least square method [31]. By inserting this T network in the cascade of Fig. 2(a) the model is now complete and can be used to analyze the UC.

C. Model Validation

To validate these models, the periodic structure is simulated using the driven modal analysis in Ansoft HFSS [30]. The complete scattering parameters of the UC are obtained and inserted into (1) after performing standard transmission line transformations [23]. The dispersion characteristic of the periodic structure using a substrate with an $\varepsilon_r = 6.15$ and $h = 250\ \mu$m is derived from (1) using the three methods and plotted in Fig. 4. A good agreement between the two models and the full-wave simulation is observed. The second model which is more accurate will be used to investigate the OSB mitigation of the UC. As it can be observed, the $n = -1$ space harmonic radiates from about 19 to 29 GHz including backward and forward regions due to negative and positive values of β_{-1}. However, this radiating region is not continuous as the radiation is highly attenuated by an OSB region where the attenuation constant increases drastically while the phase constant has an almost constant value of zero.

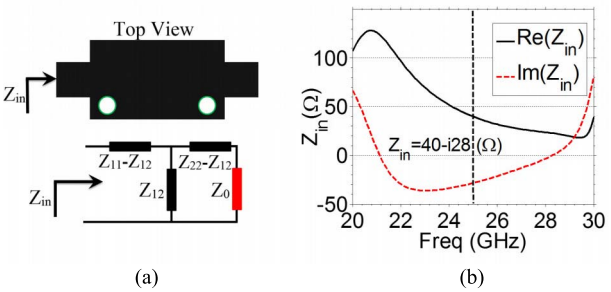

(a) (b)

Fig. 5. (a) Nonoptimized UC and its equivalent T network. (b) Input impedance of the nonoptimized UC.

D. OSB Elimination

It has been demonstrated in [9] that a matched UC will not have an OSB. To find the matched structure, the impedance matrix of the UC is extracted to obtain the TEN as shown in Fig. 5(a). If the right side of this network is terminated by the characteristic impedance of the line, Z_0 (which is 50 Ω for this structure), the input impedance can be calculated using

$$Z_{\text{in}} = [((Z_0 + Z_{22} - Z_{12})||Z_{12})] + Z_{11} - Z_{12}. \quad (5)$$

The result is shown in Fig. 5(b). As it can be observed, the input impedance has a real part which is almost equal to Z_0, and a relatively high imaginary part in the whole frequency range. This complex value of the input impedance means that the UC is not matched with the line causing the degradation of the radiation pattern. This is due to the Bloch impedance which will have a high imaginary part value and a nonconstant real part at broadside [9]. By varying the dimensions of the structure, an optimized structure can be found that has almost real input impedance. The dispersion characteristics of the optimized UC and its input impedance are shown in Fig. 6. This figure demonstrates a phase and attenuation constant without the OSB and an input impedance which has an imaginary part close to zero. The final dispersion characteristics of the UC are obtained using five cascaded cells in order to account for the coupling effects between the cells [32]. We can observe that the OSB is completely removed and the phase constant varies in a quasi linear fashion passing through broadside at 25 GHz. This will result in a continuous gain scanning from 19 to 29 GHz.

To increase the impedance bandwidth of the periodic LWA, the UC, as the radiating element, is self-matched matched with $Z_0 = 50\ \Omega$ over the desired frequency band. By doing this, we ensure that the periodic repetition of the UCs will still be matched over the bandwidth. If the matching of the UC is achieved with a small bandwidth structure, such as a matching stub, the impedance bandwidth of the UC will be limited and therefore that of the periodic LWA.

E. Scanning Range Limitations

The single beam radiation is mainly limited by the requirement that only one space harmonic must exist inside the radiation region which in our case is the $n = -1$ space harmonic. Otherwise grating lobes will appear. This requires

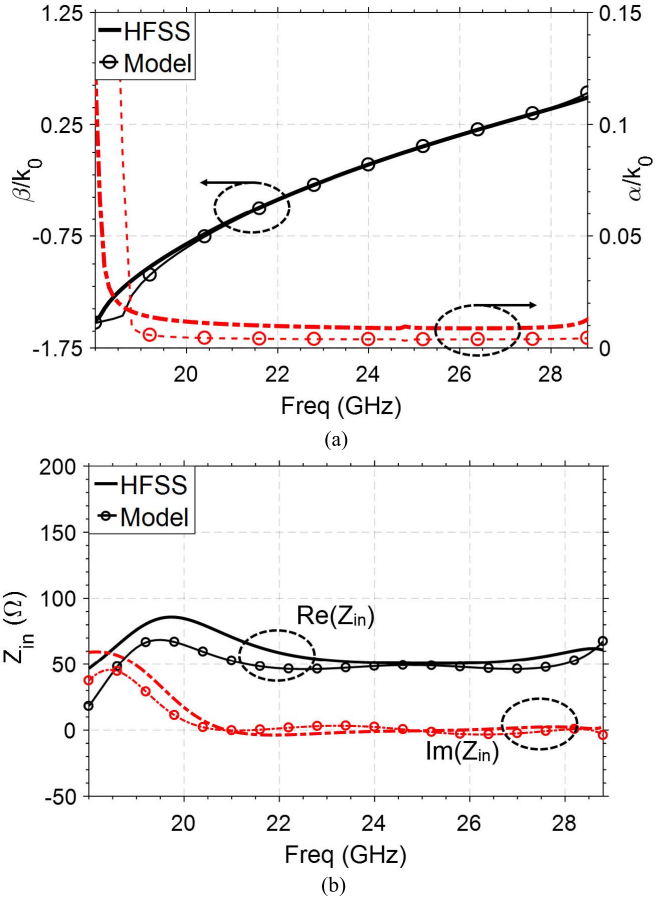

Fig. 6. (a) Normalized dispersion characteristics of the matched UC with $\varepsilon_r = 6.15$ and $h = 0.254$ mm. The solid lines represent the phase constant and the dashed lines represent the attenuation constant. (b) Input impedance of the matched UC, the solid lines represent the real part of the input impedance, and the dashed lines represent the imaginary part. ($L_1 = 3.4$, $L_2 = 1$, $W_1 = 1$ $W_2 = 2.68$, $d = 0.4$, $s = 0.9$, and $P = 5.4$ mm).

that $\beta_{-2} < -k_0$ and $\beta_0 > k_0$ when β_{-1} is in the radiation region [3].

The relative permittivity of the substrate also affects the scanning sensitivity of the periodic LWA with frequency [5], [6]. Higher values of ε_r increases the scanning sensitivity of the β_{-1} with frequency. A wide scanning range is required in several scanning applications where it is needed to be able to scan the space throughout the entire frequency bandwidth. The relatively low ε_r chosen for this structure results in a higher fundamental group velocity which in turns lowers the scanning sensitivity of the antenna (i.e., the slope of β). This allows the scanning being performed over a larger frequency range and leads to higher antenna efficiency. However, there is a limitation for the minimum value of relative permittivity that can be chosen for this purpose and it is imposed by the $n = -2$ space harmonic that must not enter the radiation region from backward directions before the $n = -1$ has finished scanning through the forward.

The dispersion diagram of the optimized UC is shown in Fig. 7. The β_{-1} space harmonic travels the radiation region from backward to forward with a high slope and reaches the limit in the forward direction before β_{-2} enters the region. It can be seen that in order to compromise for a lower

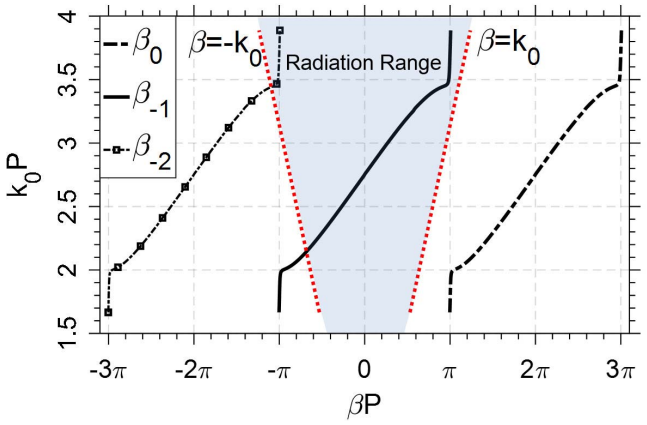

Fig. 7. Dispersion diagram of the optimized UC showing the space harmonics and the radiation range.

permittivity and a less frequency sensitivity, the radiation is degraded near the forward endfire. Not only would higher permittivity have solved this radiation issue but also it would have increased the frequency sensitivity, which is not desirable if we want to scan continuously through the whole bandwidth.

III. Antenna Design

A. Parametric Study

In order to complete our understanding on the effect of different geometrical variations on the behavior of the periodic LWA, a parametric analysis study of the UC has been performed using full-wave simulation with Ansoft HFSS [30]. This study is presented in this section.

The attenuation constant is displaced by varying L_1 due to the modification of the resonant frequency of the UC. Larger value of L_1 lowers the resonant frequency and consequently downshifts the attenuation constant as shown in Fig. 8(a). It has been observed that the distance between the two vias should be equal to $\lambda_g/2$ which is also the distance of the vias from the radiating border.

W_2 variations affects the impedance of the wider line and therefore the matching of the UC. As seen previously, in order to mitigate the OSB, the UC needs to be matched with the characteristic impedance of the line. W_2 affects this impedance matching. Moreover, by increasing W_2, the length of the radiating edge is increased and the resonant frequency is lowered. Therefore, by varying this parameter, the impedance matching of the UC and the resonant frequency can be tuned as shown in Fig. 8(b). This feature can be used to adjust the matched structure for different frequencies and attenuation constants.

Based on these two parameters the optimized matched structure can be found by first adjusting the center frequency of the structure using L_1 and then removing the OSB by matching the UC to the characteristic impedance of the line by varying W_2.

The distance of the via from the center affects the level of the attenuation constant. If we consider the high impedance line fixed, the more the vias are moved closer to the center, the higher the attenuation constant will be as depicted in Fig. 8(c). This is because of the vias getting more in the way of the propagating wave and causing more radiation. However, the distance of $s + W_2/2$ (distance of the vias to the radiating edge) needs to always remain $\lambda_g/2$ to keep the matched structure at the desired resonant frequency. Hence, a good practice is to vary this parameter by only displacing the high impedance line. This effect allows us to control the value of the attenuation constant and consequently the distribution of aperture illumination along the periodic structure. This will be discussed in Section III-C.

This parameter study reveals important physical behaviors of the structure that can be used to control the design of the antenna for different frequencies and different applications.

Moreover, it will be of crucial importance for the design of the tapered structure to modify the aperture illumination along the antenna length while keeping the periodic structure without OSB.

B. Design Process

A periodic LWA can be analyzed as an array of series fed radiators. Therefore, in order to theoretically predict the radiation behavior of the antenna from a single UC, a generalized array factor method is proposed in [33]. In this method, the leaky wavenumber which is obtained in the previous section ($k_{\rm lw} = \beta_{-1} - j\alpha$) is used to obtain the array factor.

The element factor is also obtained using the full-wave simulator. Hence, the E-plane radiation pattern ($\varphi = 90°$) of the series fed array antenna can be obtained using

$$E(\theta) = \left(\sum_{m=1}^{M} A_m e^{j\xi_n} e^{jk_0 \sin\theta z_n}\right) \times \mathrm{EF}(\theta), m = 1, 2, \ldots, M$$

$$A_m = P_m \sqrt{\alpha_m} \exp(-\sum_{i=1}^{n-1} \alpha_i P_i), \quad m = 1, 2, \ldots, M$$

$$\xi_n = \sum_{i=1}^{n-1} \beta_i P_i, \quad i = 1, 2, \ldots, N. \tag{6}$$

In (6), EF(θ) is the element pattern (which can be assumed identical for all the UCs), α_m and β_i are the attenuation and phase constants of each UC, respectively, P is the length of the UC, and z_n is the center position of the nth UC.

The final uniformly distributed LWA is simulated with a full-wave simulator [30] by combining 15 optimized UCs. The total length of the antenna is 91.5 mm which is more compact compared with similar antennas in [6]. The antenna is excited at one end and connected to a matched load at the other end.

In the case of UCs with the same dimensions, (6) can be simplified to

$$E(\theta) = \left(\sum_{m=1}^{M} A_m e^{jk_0(m-1)P\sin\theta}\right) \times \mathrm{EF}(\theta)$$

$$A_m = \exp(-jk_{lw}[(m-1)P - L/2], m = 1, 2, \ldots, M \tag{7}$$

where L is the total length of the antenna.

C. Antenna Tapering

Due to the limited length of the structure and the uniform UC the radiation pattern of the antenna possesses side lobes.

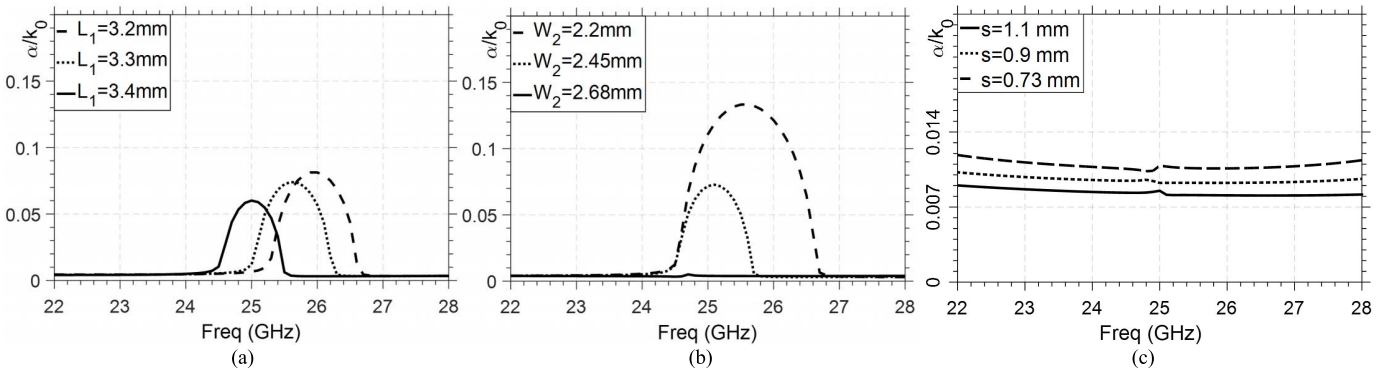

Fig. 8. Parametric study of the UC. (a) L_1 variations. (b) W_2 variations. (c) s variations.

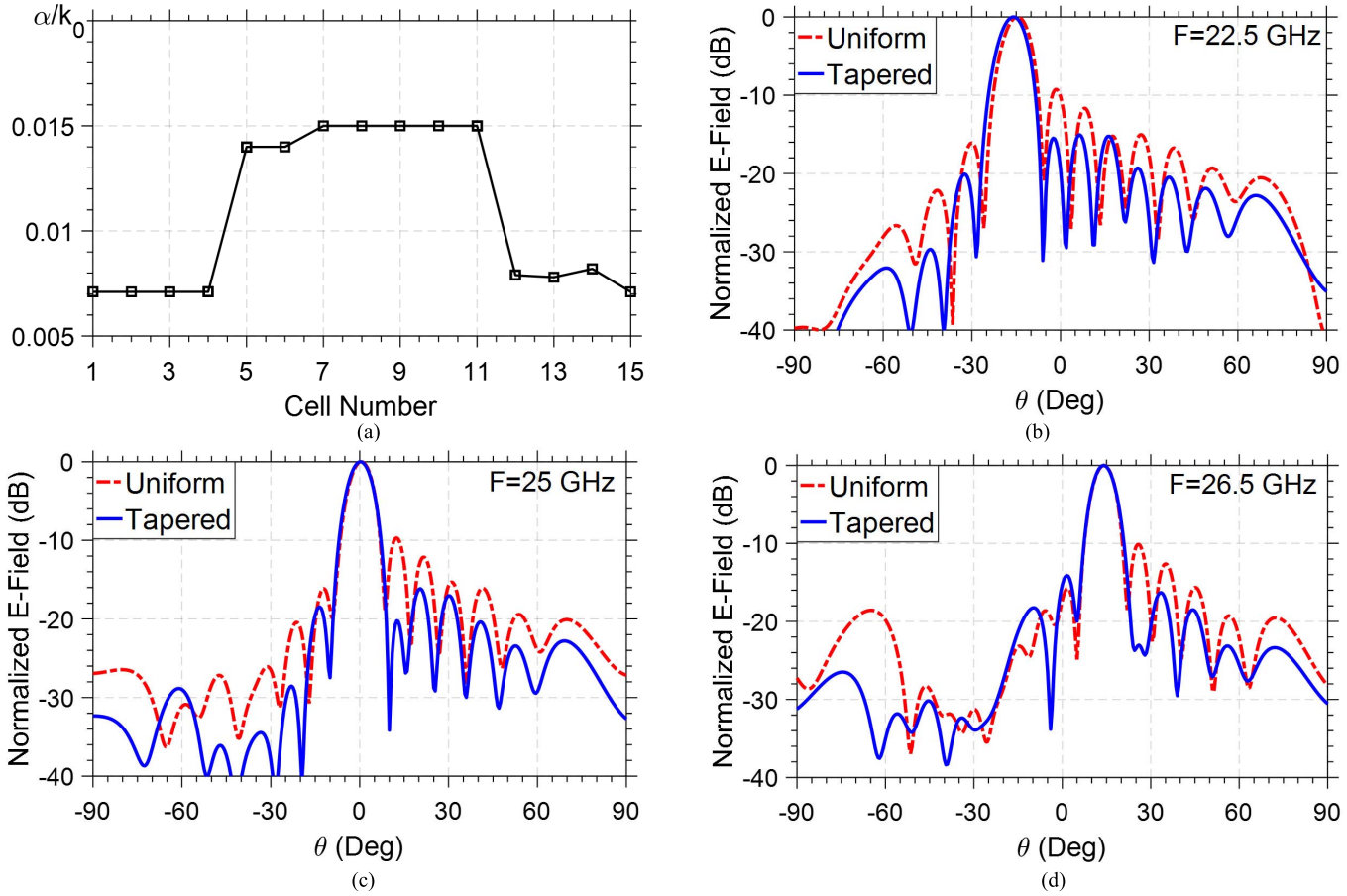

Fig. 9. (a) Normalized attenuation constant distribution of the tapered antenna (UCs are numbered from left to right). (b)–(d) Normalized simulated E-plane gain of the uniform and tapered antenna for $F = 22.5$, 25, and 26.5 GHz.

To reduce the SLL of the radiation pattern, the amplitude of the aperture distribution can be tapered. This is performed by varying the attenuation constant of the LWA for each UC while maintaining its phase constant stable [1]. In order to maintain the SLL off-broadside, each UC that we have used in this configuration needs to have a similar β/k_0 with the same slope and passing through broadside at the same frequency. At the same time, they should maintain an almost constant α/k_0 over the scanning range.

To find the tapering dimensions of the antenna, first the aperture distribution is obtained using the desired SLL. Due to the limitation of the achievable α/k_0, distributions such as Cosine or Taylor cannot be used. These distributions would require values of α/k_0 that are not possible to obtain with our UC. Hence, an iterative algorithm, such as particle swarm optimization (PSO) [34], where constraints on the result domain and fitness function can be imposed needs to be used. We have combined the PSO optimization method, with -20 dB SLL goal, and (6) to find the attenuation constant distribution as a function of the UC number. The result is shown in Fig. 9(a).

The design of an optimized periodic LWA that has low SLL and good matching performance requires independent adjustment of each UC. First, the desired attenuation constant is obtained by varying the distance of the vias from the

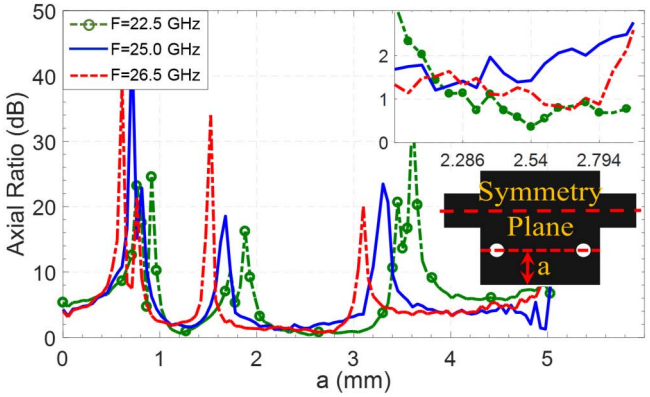

Fig. 10. Axial ratio versus a (mm) for off-broadside region and broadside.

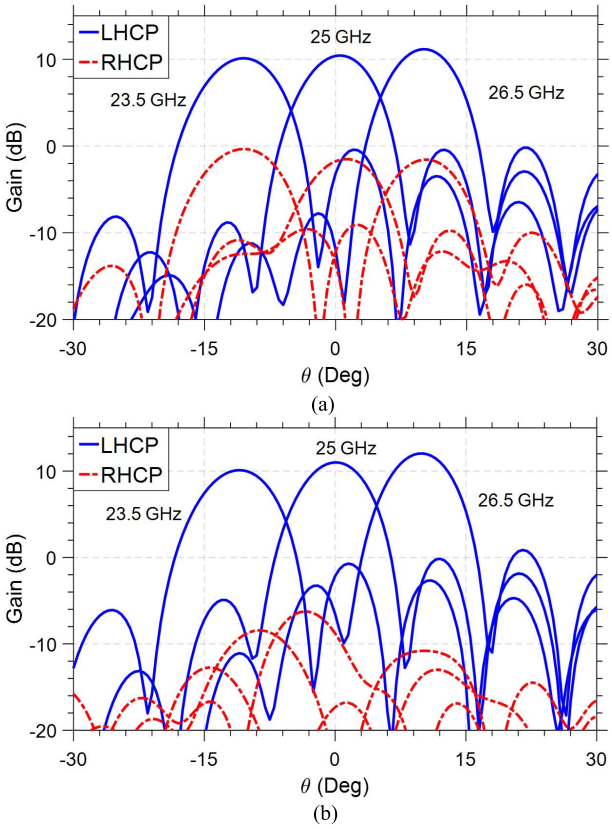

Fig. 11. Simulated co-polarization (left hand circular polarization) and cross-polarization (right hand circular polarization) for three frequencies 23.5, 25, and 26.5 GHz. (a) Before optimization. (b) After optimization.

center or by sliding the high impedance line closer or farer from the vias. The achievable attenuation range is limited by the physical size of the UC and it is possible that the required value is not achievable. The closest available value should then be selected. The position of the OSB will be slightly different in each cell as the position of the vias modifies the center frequency of the OSB (which means that β_{-1}/k_0 is displaced); by adjusting the values of W_2 the UC is matched, the OSB is suppressed, and the center frequency can be repositioned. By using this procedure for each cell, we can have a set of UCs with different attenuation constants and the same phase constant at the center frequency without any stopband. Finally,

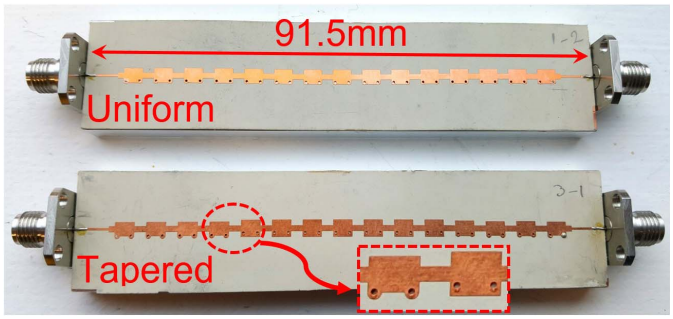

Fig. 12. Fabricated antennas mounted on an aluminum base structure.

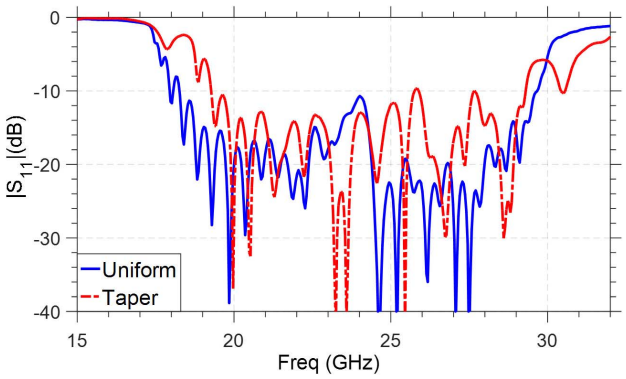

Fig. 13. Amplitude of S_{11} for two fabricated antennas.

using (6) and the values of attenuation and phase constants for each UC, the final radiation pattern of the periodic LWA can be predicted. By cascading the UCs according to this discretization, the final desired tapering is obtained.

The uniform and tapered antennas were simulated with Ansoft HFSS [30] and the comparison between the normalized gains before and after tapering is shown in Fig. 9(b)–(d) for three different frequencies. As seen, the SLL is reduced to about -17 dB at broadside. This reduction is more or less respected off-broadside and shows the effectiveness of the tapering method. However, the desired -20 dB SLL is not achieved due to the limitations of the achievable attenuation constant caused by physical boundaries of the UC.

D. Asymmetry and Circular Polarization

According to [20], the axial asymmetry in the UC produces an elliptical polarization which is due to the quadrature phase relationship between the series and shunt radiation contributions. In the optimized case, the axial ratio is close to zero dB providing a circular polarization.

In this proposed structure, due to the placement of the vias on one side of the UC, there is an axial asymmetry which produces an elliptical polarization. The axial ratio of the uniform antenna has been obtained from full-wave simulations with a value of 8 dB which verifies the elliptical polarization of the antenna. In order to optimize the axial ratio, it is proposed in [20] to adjust the asymmetry in such a manner to reach the Q-balanced state. Since the position of the via with respect to the longitudinal axis of the UC affects the broadside radiation performance of the antenna, it does not represent an

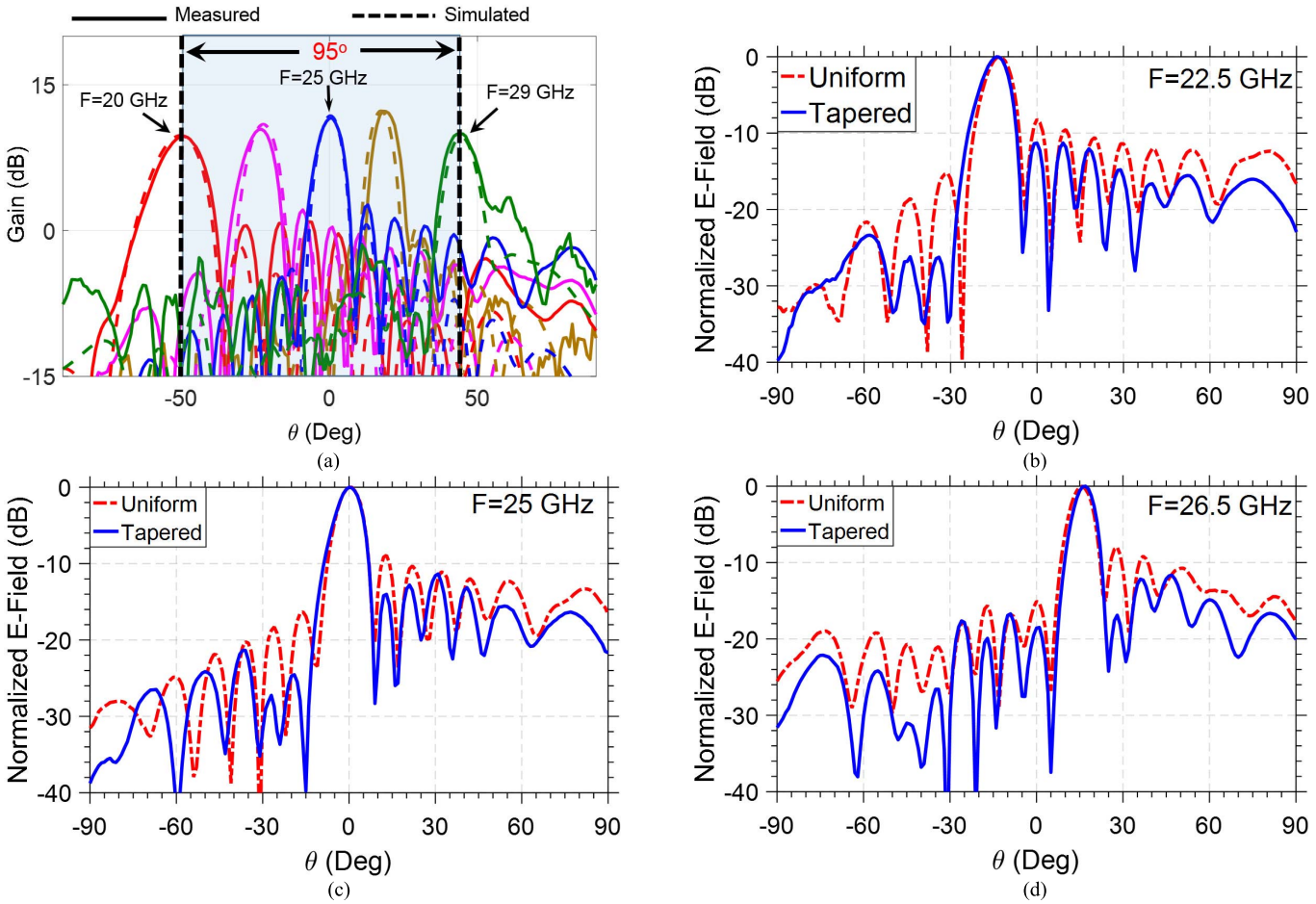

Fig. 14. (a) Measured and simulated antenna E-plane gain scanning of the uniform antenna for different frequencies. (b)–(d) Measured Normalized E-plane gain of the uniform and tapered antennas for $F = 22.5$, 25, and 26.5 GHz.

independent variable for controlling the asymmetry level and therefore the axial ratio. The position of the high impedance line also needs to be fixed as its distance from the via affects the propagation characteristics of the antenna. To investigate properly the tradeoffs between axial ratio and asymmetry degree we have found the parameter "a" which extends the UC only in one side without modifying the position of the high-impedance line and the vias with respect to the axial symmetry line as shown in Fig. 10.

Full-wave simulations were performed for "a" varying from 0 to λ_g at 22.5 and 26.5 GHz for off-broadside, and 25 GHz for broadside and results are presented in Fig. 10. Three main peaks are observed in this graph. By increasing "a" the width of the UC is increasing causing higher order modes moving in the desired frequency band. Each time a stopband produced by a higher order mode reaches our desired broadside frequency, the radiation drops and the axial ratio increases abruptly. By further increasing "a" this stopband is moved outside of the desired bandwidth and a constant leakage constant is achieved. However, it can be observed that from 0 to about 2.5 mm the axial ratio decreases by increasing the degree of asymmetry. The minimum axial ratio for the antenna is obtained at around $a = 2.3$ mm with and axial ratio of 1.3 dB around broadside which shows an almost circular polarization. It has to be noted that by further increasing the asymmetry parameter, the axial ratio is not minimized anymore. This is because with larger widths, several modes are excited at the desired frequency and we cannot move the stopband produced by one mode outside of the radiation region before another stopband appears. The axial ratio in the off-broadside region is also shown in Fig. 10. In general, it has the same behavior as the broadside with three drastic peaks and ascending rate with increasing "a" up to about 2.5 mm.

For the three regions, values of "a" between 2 and 2.5 mm provide the minimum value of axial ratio of around 1 dB which is an almost circular polarization. The cross-polarization of the antenna before and after optimization is shown in Fig. 11. As it can be observed, before the optimization the antenna has a cross-polarization rejection of about -10 dB at broadside and about the same value off-broadside. After optimizing the UC by setting $a = 2.44$ mm, the cross-polarization rejection level is about -20 dB which is suitable for various applications. Moreover, it has to be noted that at broadside frequency, if the OSB is not mitigated, the main radiation component (E_y) is severely degraded and the cross-polarization rejection level is lowered. Hence, for the whole optimization process of the axial ratio and cross-polarization, the OSB needs to remain suppressed.

TABLE I
COMPARISON WITH OTHER PERIODIC MICROSTRIP ANTENNAS

Structure	Antenna Type	Constant Gain Scanning Range (Degree) (3 dB variation over the band)	Total Length (λ_0)	Impedance Bandwidth (%)	Broadside SLL (dB)	Relative Permitivity (ε_r)
[36]	Microstrip	38	5.5	17	-10	7.8
[22]	Microstrip	70 (Normalized Gain reported)	Not Reported	6	-12	2.4
[6]	Microstrip	60	15	83	-16	2.94
[37]	Microstrip CRLH	47	5.87	61	-10	2.2
[10]	Microstrip	12 (Simulation result)	Not Reported	Not Reported	-10	10.2
[5]	Half mode SIW (X band)	86	Not Reported	34	-12	10.2
[38]	Half mode SIW (X band)	100	6	58	-9	2.2
Current work	**Microstrip**	**95**	**7.6**	**47**	**-13**	**6.15**

IV. FABRICATION AND MEASUREMENT

In order to validate the proposed structure, two antennas have been fabricated on a RO3006 substrate with $\varepsilon_r = 6.15$ and a thickness of 0.25 mm: the uniform and the tapered design. The antenna is then mounted on an aluminum base and 2.92 mm connectors are soldered at each end. The radiation patterns are then measured in an anechoic chamber. A photograph of the fabricated antennas mounted on the aluminum base is shown in Fig. 12.

The return loss has been measured using a test fixture and the result is depicted in Fig. 13. A good performance of the return loss can be observed over the desired frequency band where $|S_{11}|$ remains below -10 dB over bandwidth.

The E-plane radiation gains are depicted in Fig. 14(a) for the uniform antenna from 20 to 29 GHz and compared with full-wave simulation. As it can be observed, the fabrication results are in good agreement with the simulation. The antenna is able to provide constant gain of about 12.2 with 2.5 dB gain variation over the bandwidth for different frequency excitations. Moreover, due to the elimination of the OSB, the radiation pattern at broadside is not degraded. The scanning range is from $-50°$ at 20 GHz to 45° at 29 GHz with 95° of scanning range. The continuous gain feature of the antenna is maintained in the fabricated model. The normalized gain of the two antennas are then compared in Fig. 14(b)–(d) at 22.5, 25, and 26.5 GHz to observe the SLL reduction of the tapered antenna at broadside and off-broadside regions. At broadside, the uniform antenna has an SLL of -9 dB while the tapering lowers the SLL to about -13 dB. The reduction is also observed off-broadside. However, the SLL is still higher than the expected value from simulations. This is due to the coupling between UCs, non-ideal precision of fabrication and measurement compared to simulation resulting in different attenuation constant over the line.

Since this structure is not optimized for low axial ratio and high cross-polarization rejection, the measured polarization results are not shown here to avoid confusion. However, it has been demonstrated that using the method presented in Section III-D, the polarization performance of the antenna can be optimized for minimum axial ratio and better polarization purity.

The antenna is compared with some of the previous works in the literature in Table I. A better performance of constant gain scanning, total length, and SLL is achieved in this paper. Although the performance of our antenna is comparable to that of the antenna presented in [37], the wider width of the half mode SIW line (6 mm compared with 2.68 mm for our proposed antenna) limits the applicability of the half mode structure in compact arrays. A wide constant gain scanning range as well as low SLL and circular polarization with a simple single layer structure are the main contributions of this paper.

V. CONCLUSION

In this paper, we have presented a new compact periodic LWA with a wide scanning range. This antenna is composed of a cascade of matched UCs along the direction of propagation in order to provide continuous scanning from $-50°$ to 45°. In order to remove the OSB, the UC has to be matched with the line characteristic impedance at the broadside. The novelty of this paper resides in its UC design which is composed of two microstrip step discontinuities and two vias in a matched structure, eliminating the necessity of any other matching circuit to remove the OSB. The self-matched structure over the desired frequency band ensures a wide impedance bandwidth of 47%. Moreover, thanks to the low scanning sensitivity over frequency of the radiation pattern provided by the relatively low relative permitivity, a wide scanning range is achieved over the frequency band.

The SLL has been minimized by tapering the distribution of the leakage constant along the LWA. The leakage constant is increased with the microstrip line moving closer to the vias and decreased by increasing their distance.

A minimization of the axial ratio has been performed via a parametric study where it was demonstrated that increasing the degree of assymetry up to a certain level can lower the value of axial ratio to obtain an optimum circular polarization.

Being optimized for various factors including bandwidth, scanning range, SLL, and circular polarization, as well as simple structure, compact size, and being needless of a complicated feeding network, this antenna is a contribution to the recent developments on planar LWA.

REFERENCES

[1] D. R. Jackson and A. A. Oliner, "Leaky-wave antennas," in *Modern Antenna Handbook*, C. A. Balanis, Ed., Hoboken, NJ, USA: Wiley, vol. 1. 2008, pp. 325–368.

[2] D. R. Jackson, C. Caloz, and T. Itoh, "Leaky-wave antennas," *Proc. IEEE*, vol. 100, no. 7, pp. 2194–2206, Jul. 2012.

[3] R. E. Collin and F. Zucker, *Antenna Theory*, vol. 2. New York, NY, USA: McGraw-Hill, 1969, pp. 259–295.

[4] M. Guglielmi and D. R. Jackson, "Broadside radiation from periodic leaky-wave antennas," *IEEE Trans. Antennas Propag.*, vol. 41, no. 1, pp. 31–37, Jan. 1993.

[5] R. Henry and M. Okoniewski, "A broadside scanning substrate integrated waveguide periodic phase-reversal leaky-wave antenna," *IEEE Antennas Wireless Propag. Lett.*, vol. 15, pp. 602–605, 2015.

[6] N. Yang, C. Caloz, and K. Wu, "Full-space scanning periodic phase-reversal leaky-wave antenna," *IEEE Trans. Microw. Theory Techn.*, vol. 58, no. 10, pp. 2619–2632, Oct. 2010.

[7] W. Hong, T.-L. Chen, C.-Y. Chang, J. W. Sheen, and Y.-D. Lin, "Broadband tapered microstrip leaky-wave antenna," *IEEE Trans. Antennas Propag.*, vol. 51, no. 8, pp. 1922–1928, Aug. 2003.

[8] S. Lim, C. Caloz, and T. Itoh, "Electronically scanned composite right/left handed microstrip leaky-wave antenna," *IEEE Microw. Wireless Compon. Lett.*, vol. 14, no. 6, pp. 277–279, Jun. 2004.

[9] S. Paulotto, P. Baccarelli, F. Frezza, and D. R. Jackson, "A novel technique for open-stopband suppression in 1-D periodic printed leaky-wave antennas," *IEEE Trans. Antennas Propag.*, vol. 57, no. 7, pp. 1894–1906, Jul. 2009.

[10] J. T. Williams, P. Baccarelli, S. Paulotto, and D. R. Jackson, "1-D combline leaky-wave antenna with the open-stopband suppressed: Design considerations and comparisons with measurements," *IEEE Trans. Antennas Propag.*, vol. 61, no. 9, pp. 4484–4492, Sep. 2013.

[11] J. R. James, P. S. Hall, and C. Wood, *Microstrip Antenna: Theory and Design*. Edison, NJ, USA: IET, 1981.

[12] S. Paulotto, P. Baccarelli, and D. R. Jackson, "A self-matched wide scanning U-stub microstrip periodic leaky-wave antenna," *J. Electromagn. Waves Appl.*, vol. 28, no. 2, pp. 151–164, Jan. 2014.

[13] S. Otto, A. Rennings, K. Solbach, and C. Caloz, "Transmission line modeling and asymptotic formulas for periodic leaky-wave antennas scanning through broadside," *IEEE Trans. Antennas Propag.*, vol. 59, no. 10, pp. 3695–3709, Oct. 2011.

[14] J. S. Gomez-Diaz, D. Canete-Rebenaque, and A. Alvarez-Melcon, "A simple CRLH LWA circuit condition for constant radiation rate," *IEEE Antennas Wireless Propag. Lett.*, vol. 10, pp. 29–32, 2011.

[15] S. Paulotto, P. Baccarelli, F. Frezza, and D. R. Jackson, "Full-wave modal dispersion analysis and broadside optimization for a class of microstrip CRLH leaky-wave antennas," *IEEE Trans. Microw. Theory Techn.*, vol. 56, no. 12, pp. 2826–2837, Dec. 2008.

[16] A. Lai, T. Itoh, and C. Caloz, "Composite right/left-handed transmission line metamaterials," *IEEE Microw. Mag.*, vol. 5, no. 3, pp. 34–50, Sep. 2004.

[17] P. Baccarelli, C. Di Nallo, S. Paulotto, and D. R. Jackson, "A full-wave numerical approach for modal analysis of 1-D periodic microstrip structures," *IEEE Trans. Microw. Theory Techn.*, vol. 54, no. 4, pp. 1350–1362, Jun. 2006.

[18] S. Otto, A. Al-Bassam, A. Rennings, K. Solbach, and C. Caloz, "Radiation efficiency of longitudinally symmetric and asymmetric periodic leaky-wave antennas," *IEEE Antennas Wireless Propag. Lett.*, vol. 11, pp. 612–615, 2012.

[19] S. Otto, A. Al-Bassam, A. Rennings, K. Solbach, and C. Caloz, "Transversal asymmetry in periodic leaky-wave antennas for Bloch impedance and radiation efficiency equalization through broadside," *IEEE Trans. Antennas Propag.*, vol. 62, no. 10, pp. 5037–5054, Oct. 2014.

[20] S. Otto, Z. Chen, A. Al-Bassam, A. Rennings, K. Solbach, and C. Caloz, "Circular polarization of periodic leaky-wave antennas with axial asymmetry: Theoretical proof and experimental demonstration," *IEEE Trans. Antennas Propag.*, vol. 62, no. 4, pp. 1817–1829, Apr. 2014.

[21] M. Danielsen and R. Jorgensen, "Frequency scanning microstrip antennas," *IEEE Trans. Antennas Propag.*, vol. 27, no. 2, pp. 146–150, Mar. 1979.

[22] C. Caloz and T. Itoh, "Array factor approach of leaky-wave antennas and application to 1-D/2-D composite right/left-handed (CRLH) structures," *IEEE Microw. Wireless Compon. Lett.*, vol. 14, no. 6, pp. 274–276, Jun. 2004.

[23] D. M. Pozar, *Microwave Engineering*. New York, NY, USA: Wiley, 1998, ch. 8.

[24] T. Itoh, Ed., *Numerical Techniques for Microwave and Millimeter-Wave Passive Structures*. Hoboken, NJ, USA: Wiley, 1989, pp. 637–692.

[25] N. Marcuvitz, *Waveguide Handbook*. Edison, NJ, USA: IET, 1951, pp. 285–287.

[26] E. F. Kuester and D. C. Chang, "Propagation, attenuation, and dispersion characteristics of inhomogeneous dielectric slab waveguides," *IEEE Trans. Microw. Theory Techn.*, vol. 23, no. 1, pp. 98–106, Jan. 1975.

[27] R. Garg, I. Bahl, and M. Bozzi, *Microstrip Lines and Slotlines*. Norwood, MA, USA: Artech House, 2013, pp. 189–194.

[28] J. Liu, D. R. Jackson, and Y. Long, "Propagation wavenumbers for half- and full-width microstrip lines in the EH_1 mode," *IEEE Trans. Microw. Theory Techn.*, vol. 59, no. 12, pp. 3005–3012, Dec. 2011.

[29] T. Itoh, Ed., *Numerical Techniques for Microwave and Millimeter-Wave Passive Structures*. Hoboken, NJ, USA: Wiley, 1989, pp. 447–571.

[30] *User's Guide—High Frequency Structure Simulator*, Ansoft, Pittsburgh, PA, USA, 2003.

[31] S. C. Chapra, *Applied Numerical Methods W/MATLAB: For Engineers & Scientists*. New York, NY, USA: McGraw-Hill, 2012.

[32] G. Valerio, S. Paulotto, P. Baccarelli, P. Burghignoli, and A. Galli, "Accurate Bloch analysis of 1-D periodic lines through the simulation of truncated structures," *IEEE Trans. Antennas Propag.*, vol. 59, no. 6, pp. 2188–2195, Jun. 2011.

[33] O. Rance, P. Lemaître-Auger, R. Siragusa, and E. Perret, "Generalized array factor approach to the assessment of discrete tapered nonuniform leaky-wave antenna," *IEEE Trans. Antennas Propag.*, vol. 63, no. 9, pp. 3868–3877, Sep. 2015.

[34] R. C. Eberhart and Y. Shi, "Particle swarm optimization: Developments, applications and resources," in *Proc. Congr. Evol. Comput.*, 2001, pp. 81–86.

[35] M. H. Rahmani and D. Deslandes, "A novel periodic microstrip leaky-wave antenna with backward to forward scanning," in *Proc. IEEE-APS Topical Conf. Antennas Propag. Wireless Commun. (APWC)*, Sep. 2015, pp. 650–653.

[36] L. Liu, C. Caloz, and T. Itoh, "Dominant mode leaky-wave antenna with backfire-to-endfire scanning capability," *Electron. Lett.*, vol. 38, no. 23, pp. 1414–1416, Nov. 2002.

[37] A. P. Saghati, M. M. Mirsalehi, and M. H. Neshati, "A HMSIW circularly polarized leaky-wave antenna with backward, broadside, and forward radiation," *IEEE Antennas Wireless Propag. Lett.*, vol. 13, pp. 451–454, 2014.

Mohammad H. Rahmani (S'13) received the B.Sc. degree in electrical engineering from Azad University, Tehran, Iran, in 2008, and the M.Sc. degree from Shahid Beheshti University, Tehran, in 2011. He is currently pursuing the Ph.D. degree in electrical engineering with the École de Technologie Supérieure, Montréal, QC, Canada.

His current research interests include the development and design of antennas for wideband wireless systems, leaky-wave antennas, and passive components for high-frequency applications.

Dominic Deslandes (S'04–M'06) received the B.Sc. degree in electrical engineering from the University of Sherbrooke, Sherbrooke, QC, Canada, in 1998, and the M.Sc. and Ph.D. degrees in electrical engineering from the École Polytechnique de Montreal, Montreal, QC, in 2001 and 2005, respectively.

From 2006 to 2007, he was a Post-Doctoral Researcher with the University of Sherbrooke. From 2007 to 2016, he was a Professor with the University of Quebec, Montreal. In 2016, he joined the École de Technologie Supérieure, Montreal, where he is currently a Professor. His current research interests include the analysis, synthesis, and integration of passive components for millimeter-wave and Terahertz systems.

Dr. Deslandes was a recipient of the Natural Sciences and Engineering Research Council Doctoral Prize in 2007 for the Best Engineering Thesis in Canada. Also, one of his papers has been recognized by the Essential Science Indicators as one of the most cited article in engineering.